Manuscript prepared for Atmos. Chem. Phys.
with version 5.0 of the LaTeX class copernicus.cls.
Date: 12 April 2013

Microphysical Process Rates and Global Aerosol-Cloud Interactions

A. Gettelman[1], **H. Morrison**[1], **C. R. Terai**[2], **and R. Wood**[2]

[1]National Center for Atmospheric Research, 1850 Table Mesa Dr., Boulder, CO, 80305
[2]Department of Atmospheric Sciences, Box 351640, University of Washington, Seattle, WA, 98195

Correspondence to: A. Gettelman
(andrew@ucar.edu)

Abstract. Cloud microphysical process rates control the amount of condensed water in clouds and impact the susceptibility of precipitation to drop number and aerosols. The relative importance of different microphysical processes in a climate model is analyzed, and the autoconversion and accretion processes are found to be critical to the condensate budget in most regions. A simple steady-state model of warm rain formation is used to illustrate that the diagnostic rain formulations typical of climate models may result in excessive contributions from autoconversion, compared to observations and large eddy simulation models with explicit bin-resolved microphysics and rain formation processes. The behavior does not appear to be caused by the bulk process rate formulations themselves, because the steady state model with bulk accretion and autoconversion has reduced contributions from autoconversion. Sensitivity tests are conducted to analyze how perturbations to the precipitation microphysics for stratiform clouds impact process rates, precipitation susceptibility and aerosol-cloud interactions (ACI). With similar liquid water path, corrections for the diagnostic rain assumptions in the GCM based on the steady state model to boost accretion over autoconversion indicate that the radiative effects of ACI may decrease by 20% in the GCM for the same mean liquid water path. Links between process rates, susceptibility and ACI are not always clear in the GCM. Better representation of the precipitation process, for example by prognosing precipitation mass and number, may help better constrain these effects in global models with bulk microphysics schemes.

1 Introduction

Aerosols have many direct, semi-direct and indirect effects on clouds. The indirect effects, or Aerosol-Cloud Interactions (ACI), result from more Cloud Condensation Nuclei (CCN) creating a population of more and smaller particles for a given amount of cloud water. This makes the clouds brighter (first indirect effect, Twomey (1977)), as well as affecting the resulting lifetime of the clouds in complex ways (second indirect or lifetime effect (Albrecht, 1989)). The effects on cloud lifetime are complex, and depend upon precipitation processes in clouds. We will focus in this paper on stratiform clouds. Convective clouds with strong vertical motions, create their own complex challenges in understanding aerosol effects (Rosenfeld et al., 2008).

Many global models of the atmosphere (General Circulation Models or GCMs) have started to treat aerosol indirect effects (e.g., Boucher and Lohmann, 1995; Quaas et al., 2008). The resulting global effects of aerosols on radiative fluxes appear larger than many observational estimates from satellites (Quaas et al., 2008) or inverse methods (Murphy et al., 2009). Satellite studies and more detailed models indicate that a likely culprit is too large a change in liquid water path with the changing drop number induced by aerosols, resulting in too large a radiative effect (e.g., Wang et al., 2012). The formation of precipitation, as a primary sink for liquid water, is critical in this process. Also important are entrainment processes (e.g. Ackerman et al., 2004; Guo et al., 2011).

The evolution of precipitation in clouds is affected by aerosols through their impact on the droplet size distribution. Increases in aerosol are seen to increase cloud drop number (Martin et al., 1994; Ramanathan et al., 2001). Increased drop number means smaller mean drop size for constant liquid water path (LWP). The result is smaller drops that do not coalesce and grow into precipitation as easily. This coalescence process (described by the stochastic collection equation) is too detailed to completely represent in bulk formulations of cloud drop size distributions. Thus, the coalescence process of precipitation formation is often represented by a parameterization of the autoconversion of cloud liquid to precipitation, while the collection process of cloud

droplets onto existing raindrops is represented by an accretion process. Most current GCMs assume a diagnostic treatment of precipitation whereby time tendencies of precipitation are set to zero and precipitation is obtained by a vertical integration of microphysical process rates. On the other hand, Posselt and Lohmann (2008) assumed a prognostic treatment of precipitation that allowed precipitation mass to persist in the atmosphere across time steps in the ECHAM GCM, and found that it shifted rain production towards accretion. Wood (2005) note that autoconversion should play a minor role in increasing drizzle water content.

The autoconversion and accretion rates are affected by changes in drop number. Autconversion is sensitive to drop number (Khairoutdinov and Kogan, 2000) while accretion rates are nearly independent of the drop number: they are only affected via the mass of condensate undergoing autoconversion. If accretion dominates over autoconversion, as observed for shallow clouds (Stevens and Seifert, 2008) and stratocumulus (Wood, 2005), this would tend to dampen the ACI: reducing the role of autoconversion, which depends on cloud drop number, reduces the effect of aerosols on cloud radiative properties (Wood et al., 2009). Consistent with this idea, the change in rain rate with respect to aerosols or drop number (called the 'susceptibility' of precipitation to aerosols following Feingold and Siebert (2009)) seems to decrease at higher liquid water paths where accretion dominates (Jiang et al., 2010; Terai et al., 2012). Complicating diagnosis however, Golaz et al. (2011) found a strong co-variance between ACI and LWP with changes in process rates to achieve radiative balance in a GCM.

In contrast to previous work on microphysics processes in GCMs (Posselt and Lohmann, 2008; Wang et al., 2012), we compare GCM process rates to rates derived from in-situ observations and we explore a simple steady state model of microphysical processes. We first examine microphysical process rates in a GCM (Section 2). We analyze a simple steady state model (Section 3) to understand interactions of process rates and susceptibility of precipitation to changes in drop number. We compare the GCM to the simple model and observations in Section 4. We then use different formulations of the GCM microphysics to better understand the sensitivity of the GCM cloud aerosol interactions in Section 5. Discussion and Conclusions are in Section 6.

2 Balance of processes in a GCM

2.1 Model Description

The GCM we use in this study is the National Center for Atmospheric Research (NCAR) Community Atmosphere Model version 5.2 (CAM5). CAM5 includes an advanced physical parameterization suite (Gettelman et al., 2010; Neale et al., 2010) that is well suited for understanding aerosol indirect effects in stratiform clouds. CAM5 has a 2-moment cloud microphysics scheme (Morrison and Gettelman, 2008; Gettelman et al., 2008), coupled to a modal aerosol model with 3 modes (Liu et al., 2012). CAM5 aerosols affect activation of stratiform cloud droplets and ice crystals. Aerosols in the standard version of CAM5 do not interact with convective cloud drops and ice crystals. A separate scheme is used to describe convective clouds and convective microphysics (Zhang and McFarlane, 1995). CAM5 has a consistent treatment of the radiative effects of cloud droplets and ice crystals, and radiatively active snow (see Gettelman et al. (2010) for details). We will also perform several sensitivity tests as noted below (see Section 5) with different CAM5 formulations.

In CAM, liquid autoconversion (auto) and accretion (accr) are defined following Khairoutdinov and Kogan (2000):

$$\frac{\partial q_r}{\partial t}_{auto} = A_u = 1350 q_c^{2.47} N_c^{-1.79} \quad (1)$$

$$\frac{\partial q_r}{\partial t}_{accr} = A_c = 67 (q_c q_r)^{1.15} \quad (2)$$

Autoconversion depends on cloud water (q_c) and inversely on cloud drop number (N_c) so that increases in drop number decrease rain rate (q_r) to a first approximation, leading to more liquid in the presence of higher number (more aerosols). Accretion depends on q_c and q_r only in this formulation. The rain mixing ratio q_r in CAM is diagnostic: only from rain formed at the current time step.

To isolate cloud lifetime and precipitation effects of aerosols in a GCM, first we examine the key CAM microphysical process rates in Figure 1. This analysis treats evaporation and condensation as large scale (macro-physical) quantities, and here we focus only on the microphysics. These terms are important in the overall amount of cloud water. We look at the storm track regions, where liquid water path is large, and in CAM there is a large sensitivity of cloud feedbacks in this region (Gettelman et al., 2012). Over the storm track regions (S. Hemisphere shown in Figure 1 A), autoconversion of liquid to precipitation, accretion of liquid by snow and the transition from liquid to ice (Bergeron process) are the largest sink terms for liquid. Autoconversion is the largest process rate from 500–900hPa, with the Bergeron vapor deposition larger below that. Accretion is lower than autoconversion. In the S. E. Pacific off the coast of S. America (Figure 1 B), there is a large sedimentation term, but the dominant microphysical processes after that are Accretion and Autoconversion. Both are nearly equal, but there is more autoconversion near cloud top (∼800 hPa). Over the Tropical Western Pacific (20S to 20N and 120–160 longitude), the dominant processes are similar. Autoconversion and accretion onto both rain and snow are the dominant sink terms for cloud liquid (Figure 1 C). Several other terms are important due to ice processes at high altitudes (homogeneous

Table 1. Description of steady state simulations.

Name	Description
Base	Base simulation
Qcv=2	Modify rates with CAM sub-grid variability
QiagQr	Different accretion: with auto converted liquid
QiagQr$^{0.5}$	DiagQr + Scaled rain mixing ratio for accretion

freezing and accretion of liquid onto snow). Accretion and autoconversion have similar magnitudes. Figure 1 shows that regardless of the cloud regime or region, accretion and autoconversion largely determine the sink of cloud liquid water.

3 Steady State Model

Given the dominance of the autoconversion and accretion processes, we explore a simple model that represents these essential features in much the same way as the GCM. We use the steady state model of Wood et al. (2009), which captures many of the qualitative and quantitative features of warm rain processes. Time tendencies of precipitation mass (and number) mixing ratios are explicitly calculated and precipitation quantities are prognosed across time steps. The model calculates an equilibrium state for rain rate, rain number and cloud water concentration given an input cloud height, replenishment rate and drop number concentration. The essential processes are autoconversion and accretion, combined with sedimentation and removal of cloud water. The model treats rain prognostically, and uses autoconversion from Khairoutdinov and Kogan (2000) as in Equation 1. We use the accretion calculation of Khairoutdinov and Kogan (2000) as in Equation 2, to be consistent with the GCM simulations, and keep all parameters the same. The standard case, seen in black in Figure 2, reproduces the sensitivity of precipitation to LWP and N$_d$ in Wood et al. (2009), their Figure 1b. Steady state model cases are described in Table 1.

The bulk microphysics in the GCM differs in several important respects from this steady state model. As described by Morrison and Gettelman (2008), the bulk microphysics treats the impact of the sub-grid variability of total water in a grid box, by assuming a standard deviation, and analytically adjusting the process rates by integrating over an assumed gamma distribution. The result, for a relative variance of 2, is an increase in autoconversion by a factor of 2.02, and of accretion by 1.04. It is straightforward to apply these terms to the steady state model (simulation Qcv=2), but the results do not change much. The precipitation rate is very similar to the base case (not shown) and the ratios between accretion and autoconversion (Figure 3 A), autoconversion and rain rate (Figure 3 B) and accretion and rain rate (Figure 3 C) are basically unchanged. The 'susceptibility' of precipitation to drop number (Figure 3 D), here defined as $S_p = -\partial \ln(\mathrm{R})/\partial \ln(N_d)$ with R being the Rain Rate, is also very similar, with slightly lower values at high LWP.

In addition, the GCM does not have rain mass and number mixing ratios that are carried from time step to time step (prognostic rain), but assumes instead that rain only depends on the prognostic cloud quantities over the model time step (typically 20-30 minutes). Thus, rain profiles are found by integration of the microphysical process rates over height but not time (diagnostic rain) as described in (Morrison and Gettelman, 2008, section 2b). In the steady state model however, rain mass mixing ratios increase over time at a given vertical level, leading to an increase in accretion. In the GCM, accretion is caused only by rain which is created (through autoconversion) diagnostically at each time step and falls through cloud water at lower levels. In order to reflect this behavior in the steady state model, we can assume that accretion is affected only through rain created at the current time step, thus:

$$\frac{\partial q_r}{\partial t}_{accr} = A_c = 67(q_c q_a)^{1.15} \quad (3)$$

Where q_a is the 'autoconverted' liquid (q_a) from the autoconversion rate ($q_a = A_u \rho dt$). This formulation (in blue in Figure 2 and Figure 3) changes the balance dramatically in the steady state model, causing a significant reduction in rain rate, and a constant relationship between the autoconversion and rain rate across all values of LWP (Figure 3 B). The accretion is much less important (Figure 3 C), and susceptibility to drop number (Figure 3 D) is increased at high liquid water paths (it does not decrease as in the standard steady state model). This is consistent with previous work (Posselt and Lohmann, 2008; Wang et al., 2012) indicating that the prognostic rain formulation reduces the impact of autoconversion. Note that q_a in Equation 3 is dependent on time step. We have tested a range of time steps from 5-30 seconds in the steady state model, and the time step does not change the susceptibility with LWP or the slope of the A_c/A_u ratio with LWP.

Next we explore ways to recover the steady state model behavior with the 'diagnostic' rain rate (only from q_a, the autoconverted liquid, as in equation 3). Boosting accretion by a factor of 10 alters the accretion/autoconversion (A_c/A_u) ratio, but not significantly (experiments with this change look identical to the diagnostic rain in Figure 3). As a second experiment, we assume that because q_r increases lower in the cloud, there is increased efficiency of accretion over autoconversion as the rain builds in the lower part of a cloud. We express this as a power law $q_{amod} = q_a^x$, where for $x < 1$ accretion is boosted (since the rain mixing ratio $q_r < 1$). For illustrative purposes, we choose x=0.5 in Figure 3 (DiagQr$^{0.5}$: blue lines). This method significantly increases the rain rate, matching the steady state model base case for moderate LWP (100-300 g m^{-2}). It also increases the accretion/autoconversion ratio (Figure 3 A) and the role

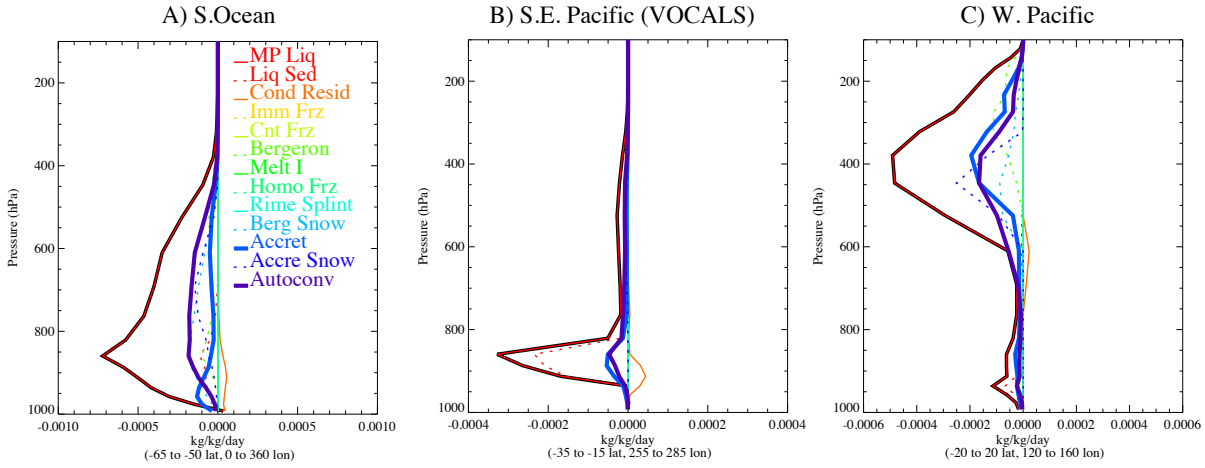

Fig. 1. Profiles of annual average grid mean liquid microphysical process rates (colored solid and dotted lines) in CAM5. A) S. Ocean (-65 to 50 lat, all longitudes), B) S. E. Pacific (-35 to -15 S and 255-285E) and C) Tropical Western Pacific (TWP: 20S to 20N and 120-160E). Processes are the total microphysical tendency (MP Liq), Sedimentation (Liq Sed) and the residual condensation to remove supersaturation (Cond Sed), Immersion freezing (ImmFrz), Contact freezing (Cnt Frz), the Bergeron vapor deposition process (Bergeron), Melting of ice (Melt I), Rime Splintering (Rime Splint), Homogeneous Freezing of cloud drops to ice (Homo Frz), Autoconversion (Autoconv), Accretion (Accret) and the vapor deposition onto snow (Berg Snow).

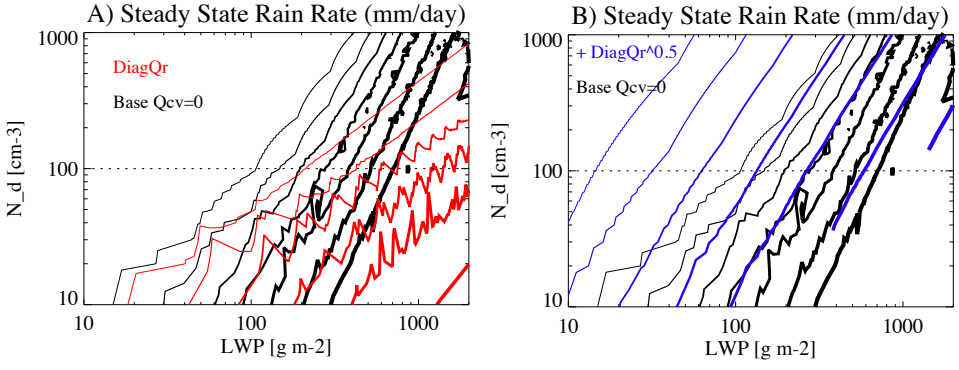

Fig. 2. Results from steady state model of Wood et al. (2009). Rain rate (mm/day), contour lines at 0.03, 0.1, 0.3, 1, 3, 10 and 30 mm day^{-1}. Thicker lines are higher rain rates. Cases shown: (A) Base case (Black) and Diagnostic rain case (DiagQr, Red). (B) Base case (Black) and diagnostic rain with vertical variation of rain rate from autoconversion (DiagQr$^{0.5}$: Blue) as described in the text.

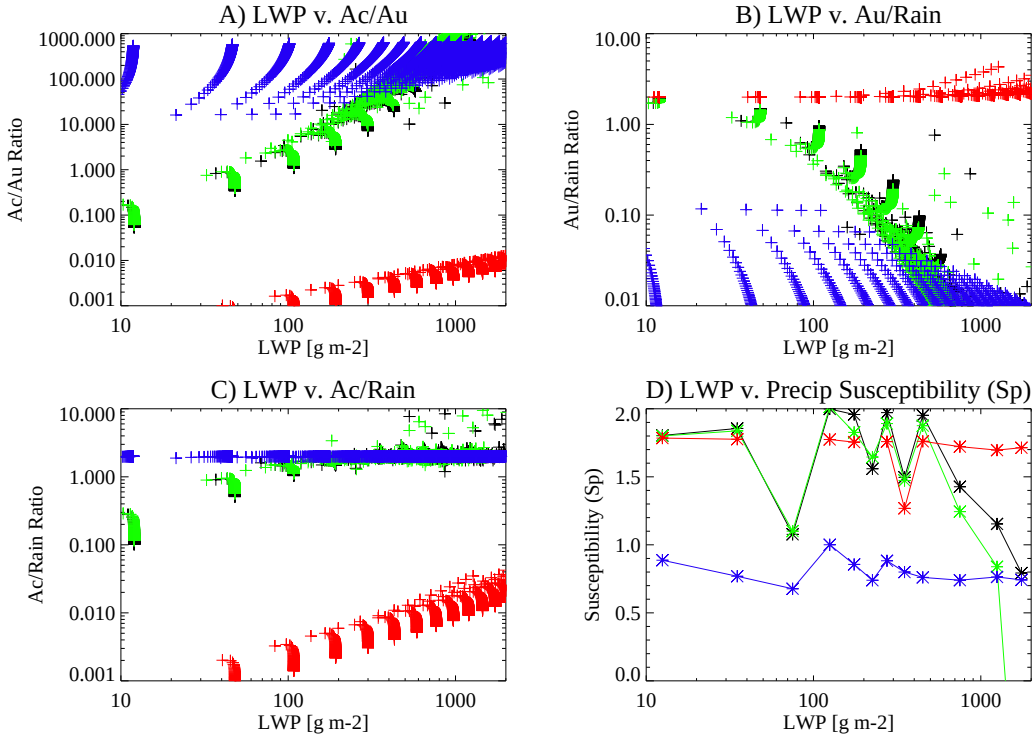

Fig. 3. Results from steady state model of Wood et al. (2009). (A) LWP v. Accretion to Autoconversion ratio (A_c/A_u), (B) LWP v. Autoconversion to Rain Rate (A_u/Rain), (C) LWP v. the ratio of Accretion to Rain rate (A_c/Rain) and (D) LWP v. Precipitation Susceptibility. Cases shown: the Base case (Black), case with sub-grid variability (Qcv = 2) in Green, Diagnostic rain case (DiagQr, Red), and diagnostic rain with vertical variation of rain rate from autoconversion (DiagQr$^{0.5}$: Blue) as described in the text.

of accretion in rain formation (Figure 3 C), and reduces the impact of autoconversion (Figure 3 B), while also uniformly lowering susceptibility (Figure 3 D). The results do not fully reproduce the base case steady state model, particularly susceptibility (S_p) with respect to varying LWP. In Figure 3 D, for the simulations that give the two extremes of A_c/A_u ratios (DiagQr$^{0.5}$ in blue and DiagQr in red), S_p is nearly constant with LWP. Note that the susceptibilities in the steady state model correspond to the exponents for Autoconversion ($\sim$1.79) for all simulations except DiagQr$^{0.5}$, where S_p is around half that of Autoconversion ($\sim$0.9). In the equilibrium model, the slope of the rain rate with specified droplet number is dominated by the exponent for autoconversion, but slightly less so when accretion dominates. These results are consistent with previous studies that susceptibility is related to the ratio between accretion and autoconversion and the A_u/R ratio (Wang et al., 2012). Note the similarity of Figure 3A (inverse) and Figure 3B with Figure 3D.

4 GCM Results

We now focus on these process rates in the GCM, analyzing the ratio of Accretion to Autoconversion (Jiang et al., 2010), the ratio of Autconversion (and accretion) to precipitation (Wang et al., 2012), and the susceptibility of precipitation to aerosols (or drop number) (Sorooshian et al., 2009; Terai et al., 2012). We composite the diagnostics by liquid water path (LWP) and by aerosol optical depth (AOD). Note that the LWP is that used in estimating microphysical process rates immediately before the microphysics calculation, not the diagnostic LWP in CAM used by the radiation code (the latter is the traditional GCM output).

4.1 Accretion/Autoconversion

The autoconversion of cloud condensate to precipitation and the accretion or collection of falling condensate by precipitation are the dominant terms in most places for the microphysical sink of cloud water (Figure 1).

Figure 4 shows zonal cross sections and maps of the autconversion and accretion rates in CAM5. As expected, autoconversion (Figure 4 D) and accretion (Figure 4 B) rates are both larger in midlatitudes than in the tropics where stratiform liquid water paths are higher. Note that these processes and diagnostics do not treat convective clouds (because the simplified convective microphysics does not have these rates), so results for the tropics need to be interpreted with caution. The ratio between accretion and autoconversion (Figure 4 E) is large in the tropical troposphere below the freezing level. Because of the different vertical altitudes and sedimentation, and because it is the vertical integral that is relevant for surface precipitation rate, the vertically averaged A_c and A_u rates (over all altitudes, but essentially just the troposphere) are used for a ratio (Figure 4 F). In CAM5, accretion (A_c) dominates with the A_c/A_u ratio typically between 1-10. The A_c/A_u ratio is lower (more autoconversion) in the mid-latitude regions where the liquid water path is high. In general, the A_c/A_u ratio is larger than 1, indicating that accretion is more important.

In LES simulations (Jiang et al., 2010), the ratio of accretion to autoconversion increases with LWP. Figure 5 shows an estimate of accretion and autoconversion rates based on observations. The autoconversion and accretion rates are estimated from the droplet size distributions measured on the NCAR/NSF C-130 during the VOCALS experiment off the west coast of South America on profile legs flown through the depth boundary layer (Wood et al., 2011). A mean droplet size distribution is calculated over ten second segments, and after interpolating any gaps in the size distribution, the mass conversion of cloud to drizzle for autoconversion and accretion is calculated using the stochastic collection equation given the size distribution following the method described by Wood (2005). The 10-second-average process rates are averaged over continuous layers of liquid water content (LWC) exceeding 0.01 gm^{-3}. The LWPs (drizzle+cloud) are estimated only over the cloud layer. A size (radius) cutoff of 25 microns is used to distinguish cloud and drizzle drops, following Khairoutdinov and Kogan (2000). Measurements of droplet size distribution come from the CDP (Cloud Droplet Probe) for the cloud drops and the 2D-C probe for drizzle drops (Wood et al., 2011). Here, the ratio of accretion to autoconversion increases sharply with LWP, as in the LES simulations.

In CAM, the ratio of accretion to autoconversion (A_c/A_u) decreases with LWP (Figure 5A), in contrast to the observations and LES models. This appears to be mostly because autoconversion increases with LWP (Figure 5B)faster than accretion (Figure 5C). The A_c/A_u ratio also decreases with increasing AOD (Figure 5D). Autoconversion increases with AOD in any region (Figure 5E), which is not what would be expected from the formulation in Khairoutdinov and Kogan (2000). It may result from the fact that LWP increases with AOD in CAM, and the convolved variables make it difficult to separate AOD-driven effects in this analysis (the positive correlation between AOD and LWP does not imply causation, just covariance). Accretion decreases with AOD (Figure 5F) in the S. Ocean and S. E. Pacific, but is nearly constant with LWP globally.

CAM has a fundamentally different relationship between the A_c/A_u ratio and LWP than seen in the steady state model in Figure 3. The A_c/A_u ratio increases with LWP (Figure 3A) in the steady state model or observationally based estimates in Figure 5. However, in the steady state model with modified accretion, following Equation 3 (DiagQr), the A_c/A_u ratio is 3 orders of magnitude lower than the basic steady state model, and increases less with liquid water path, similar to the GCM.

4.2 Precipitation and Autoconversion

To investigate the impact of microphysical processes and aerosols on precipitation, we look at the non-dimensional ratio of the vertical integral of autoconversion (A_u) or accretion (A_c) to the rain rate (R) in Figure 6. Previous studies (e.g., Wang et al., 2012) note that that the autoconversion/rain ratio is important in determining LWP response to CCN. In drizzling stratocumulus, this ratio is small (Wood, 2005). Wang et al. (2012) highlight that the precipitation occurrence is related to the A_u/R ratio (since autoconversion is the initial formation of precipitation), whereas the precipitation amount is more dependent on the accretion process and the A_c/R ratio. Note that in CAM, there is an additional avenue for rain formation that is not accounted for in this analysis of autoconversion and accretion (for liquid): and that is the formation of frozen precipitation (snow) that melts to form rain. Hence there can be zero autoconversion or accretion for a non-zero rain rate in this analysis.

In Figure 6 from the GCM, the A_u/R ratio increases with LWP, from 0.0 to 0.7 globally (Figure 6A). There does not appear to be a clear relationship between the A_u/R ratio and AOD (Figure 6C). The A_c/R ratio increases rapidly and then decreases with increasing LWP (Figure 6B) and decreases in many regions with higher AOD (Figure 6D). The A_u/R and A_c/R ratios need not add to one (i.e. $A_c + A_u \neq R$) because of the evaporation of precipitation (sum > 1) or ice phase processes (sum < 1). These ratios from CAM are consistent with other work (Wang et al., 2012). Autoconversion/rain ratios are much higher than seen in embedded cloud resolving model simulations by Wang et al. (2012), and in stratocumulus observations by Wood (2005), where autoconversion played a smaller part in determining rain rates. The A_u/R ratios (Figure 6A) are very different from those in the steady state model with prognostic rain (Figure 3 B, red and black), where the A_u/R ratio decreases with LWP. The GCM A_u/R ratio is more consistent with the increase in A_u/R ratio with LWP in steady state model simulations using modified accretion (Figure 3 B, blue). The relationship between accretion and rain rate is also very different in the steady state model

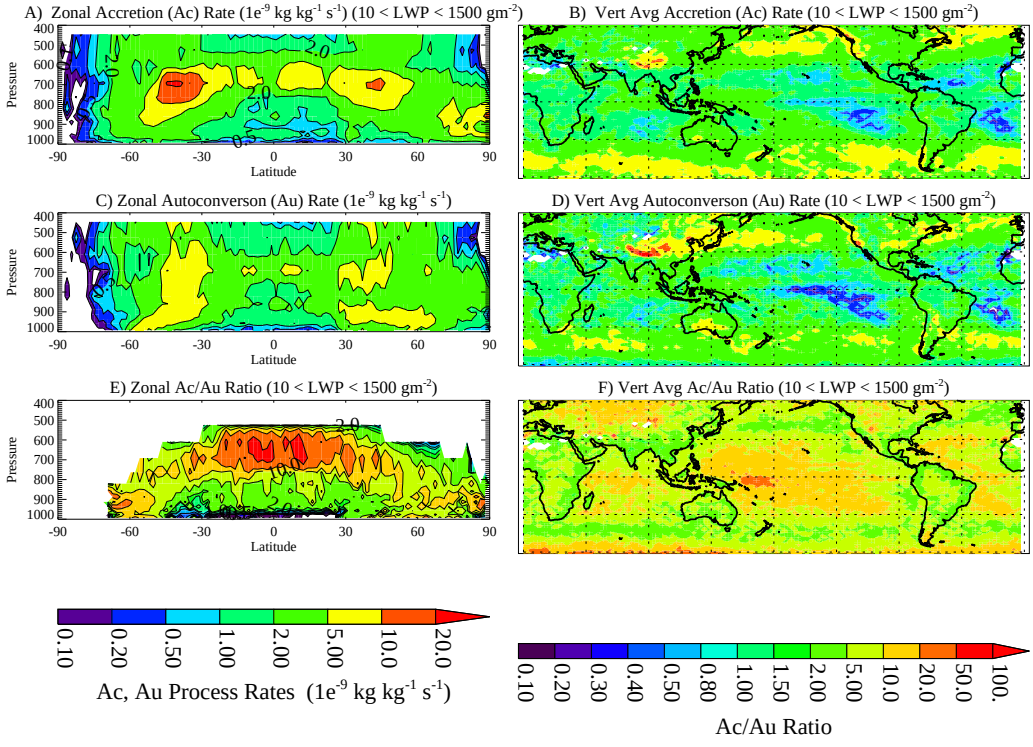

Fig. 4. Zonal mean latitude height (A,C,E) and vertically averaged maps (B,D,F) of Accretion rate (A_c: A,B), autoconversion rate (A_u: C,D), and the ratio of accretion to autoconversion rate (A_c/A_u: E,F) for all Liquid Water Paths.

(Figure 3 C): where accretion increases relative to rain rate for increasing LWP, but decreases in the GCM (Figure 6C).

4.3 Precipitation Susceptibility

The susceptibility of precipitation (S_p) to aerosols is a part of the cloud lifetime effect (Jiang et al., 2010; Feingold and Siebert, 2009). S_p is defined in the GCM similarly to the steady state model, but using the column cloud drop number (CDN) concentration for N_d. Thus, S_p= -∂ln(R)/∂ln(CDN). In the GCM, we look at instantaneous output from the model at each point, and consider only points with significant (>5x10^{-9} kg m^{-2} s^{-1}) rain rates. The output is binned by region and LWP, and then slopes are calculated. In LES simulations of trade cumulus by Jiang et al. (2010), when binned by LWP, susceptibility increases with LWP, and then decreases at high (LWP $>$ 1000 gm^{-2}). Terai et al. (2012) find only decreasing S_p with LWP in drizzling stratocumulus when non-drizzling profiles were included. Terai et al. (2012) found no change in S_p with LWP when only drizzling cases were examined. In the steady state model (Figure 3 D), S_p is generally constant and then decreases for high LWP, but not for the case with altered accretion formulation (DiagQr), where there is higher susceptibility at high LWP (Figure 3 D, blue).

Figure 7 indicates that in CAM5, precipitation susceptibility to drop number (S_p) increases with LWP. At high LWP, S_p decreases modestly in some regions. This relationship is different from S_p values reported by previous studies (Jiang et al., 2010; Terai et al., 2012), or the steady state model results (Figure 3). Because of scatter, the quantitative values of S_p are lower than in the steady state model (Figure 3 D). The high values of susceptibility at higher LWP are consistent with the results above showing a strong impact of autoconversion on rain rate at higher LWP (Figure 6A), since the autoconversion depends on drop number, changes in drop number will have a large impact on autoconversion and hence rain rates.

Maps of S_p in CAM for warm rain (Figure 8), composited by LWP, illustrate that at low and moderate LWP, patterns are fairly uniform, and susceptibility is low (Figure 8A and B). At high LWP (Figure 8C), precipitation susceptibility (S_p) is larger over the sub-tropical equatorward parts of the oceanic storm tracks. At high LWP (Figure 8C), S_p is higher

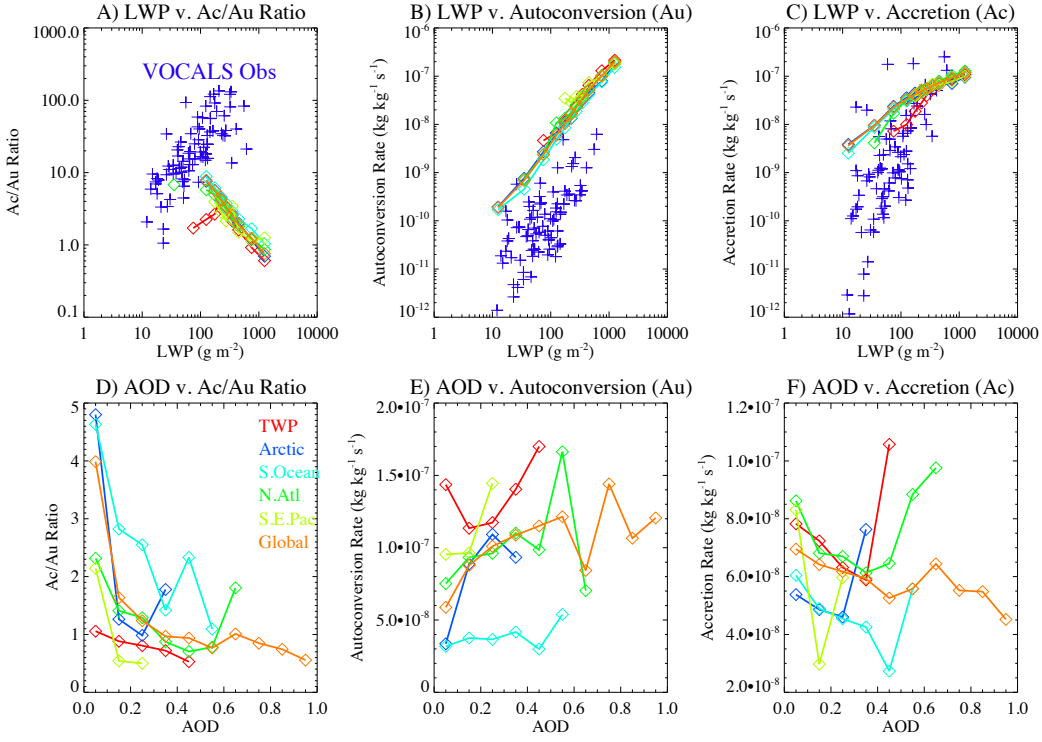

Fig. 5. Regional and global averages of vertically averaged (A) Accretion/Autoconversion (A_c/A_u) ratio v. LWP , (B) Autoconversion (A_u) rate v. LWP and (C) Accretion (A_c) rate v. LWP. Also shown are (D) A_c/A_u ratio, (E) (A_u and (F) A_c v. AOD. Regions correspond to: Tropical Western Pacific (TWP: 20S–20N, 120–160E), Arctic (65N–80N, all longitudes), S. Ocean (65S–60S, all longitudes), N. Atlantic (40N–60N, 300–360E), S. E. Pacific (30S–10S, 260–295E), and Global.

in the N. Pacific and the SH storm track than over land. S_p is lower over land at moderate and high LWP. This is consistent with the A_c/A_u ratio being lower (more autoconversion) over oceanic storm tracks (Figure 4F) where the susceptibility (S_p) is higher (Figure 8C).

We have also looked at the ratio of the timescales for drizzle (τ_{driz}) and condensation (τ_{cond}) in the GCM. These are defined following Wood et al. (2009) as $\tau_{driz} = q_l/(A_c+A_u)$ and $\tau_{cond} = q_l/A_{cond}$ where A_{cond} is the total condensation rate. Wood et al. (2009) found τ_{driz}/τ_{cond} to be a good predictor of susceptibility (S_p). We do not see strong relationships between τ_{driz}/τ_{cond} and S_p. In general τ_{driz}/τ_{cond} is low, and condensation dominates. Unlike the steady state model, τ_{driz}/τ_{cond} does not seem to determine the susceptibility (S_p) in the GCM.

5 Global Sensitivity Tests and ACI

5.1 Experiments

We now examine how changes to the model formulation affect process rates and aerosol indirect effects. Experiments are listed in Table 2. Each experiment is a pair of simulations, run for five years at 1.9x2.5 horizontal resolution with fixed year 2000 climatological SSTs and year 2000 greenhouse gas concentrations. One experiment uses year 2000 emissions, and the other 1850 emissions. SSTs and GHGs are the same in both. We have thus far shown results from the year 2000 base simulation.

Aerosol emissions for either present day (2000) or 'pre-industrial' (1850), are from Lamarque et al. (2010). These are the same emissions used in the Coupled Model Intercomparison Project phase 5 (CMIP5) (Taylor et al., 2012). Aerosol indirect effects (ACI) are estimated by looking at the Radiative Flux Perturbation (RFP) in pairs of simulations with different aerosol emissions. CAM5.2 has an aerosol in-

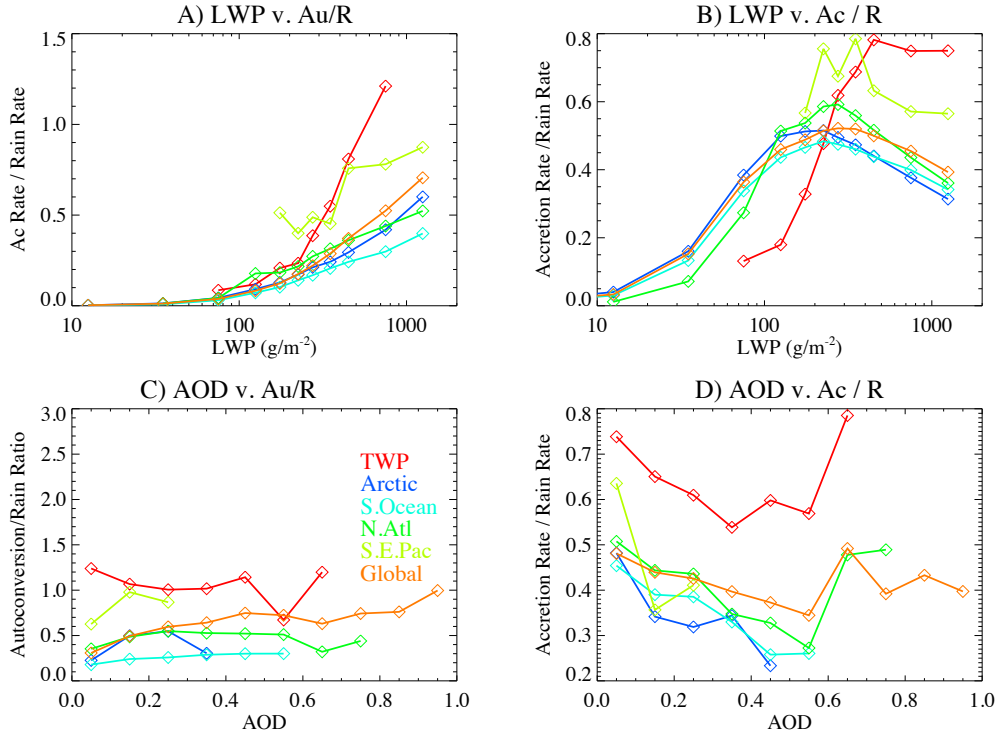

Fig. 6. Regional averages of the ratio of (A,C) autoconversion and (B,D) accretion to surface precipitation rate for different regions (colors, see Figure 5 for description) binned by (A,B) LWP and (C,D) AOD.

direct effect for liquid clouds of -1.4 Wm^{-2} and +0.4 Wm^{-2} for ice (Table 3).

Based on the results of the steady state model tests, we construct several different modifications to the microphysical process rates from the base model in section 4. In one experiment, we reduce autoconversion by a factor of 10 (Au/10). In another we increase accretion by a factor of 10 (Ac*10), and in a third we scale the rain mixing ratio for accretion by an exponent of 0.75 ($QrScl^{0.75}$). The $QrScl^{0.75}$ simulation is similar to the $DiagQrl^{0.5}$ steady state model experiment. In order to ensure that the level of liquid water in the simulated clouds does not decrease too much, we also scale back autoconversion in this simulation by a factor of 10.

We also explore the impact of the coupling between condensation and microphysics in the simulations by reducing the time step by a factor of 4 from 1800 to 450s (dT/4). The dynamics time step in the CAM5 finite volume core in standard (dT = 1800s) simulations is sub-cycled 4 times, and this sub-stepping is set to 1 in the dT/4 simulation, so the dynamics has a similar effective time step, but the physics is running with a shorter time step (and affecting the dynamics more often). There are many couplings between the different physical processes that are altered in this simulation, so this is not a clean experiment for changing the microphysics time-step. The intent is to try to reduce the amount of time for microphysics to deplete the condensation which occurs. We also perform an experiment where A_c is increased (*10) and A_u lowered (/10) so that LWP is nearly constant (AcAu2). This experiment used a slightly different code (on a different supercomputer) so it is comparable only to its own base case (Base2). These cases are detailed in Table 2.

5.2 Global Results

First we report basic statistics for the radiative and precipitation impact of anthropogenic aerosols in the CAM5 simulations. Table 3 shows differences (2000-1850) from the different aerosol emissions in the simulations. The total aerosol effect is the Radiative Flux Perturbation or RFP, the change in top of atmosphere net radiative flux (RFP=dR). The quantitative radiative indirect effect (or ACI) can be isolated in several ways, following Gettelman et al. (2012). The change in cloud radiative effect (dCRE) is representative of the indirect effect and can be broken into LW and SW components.

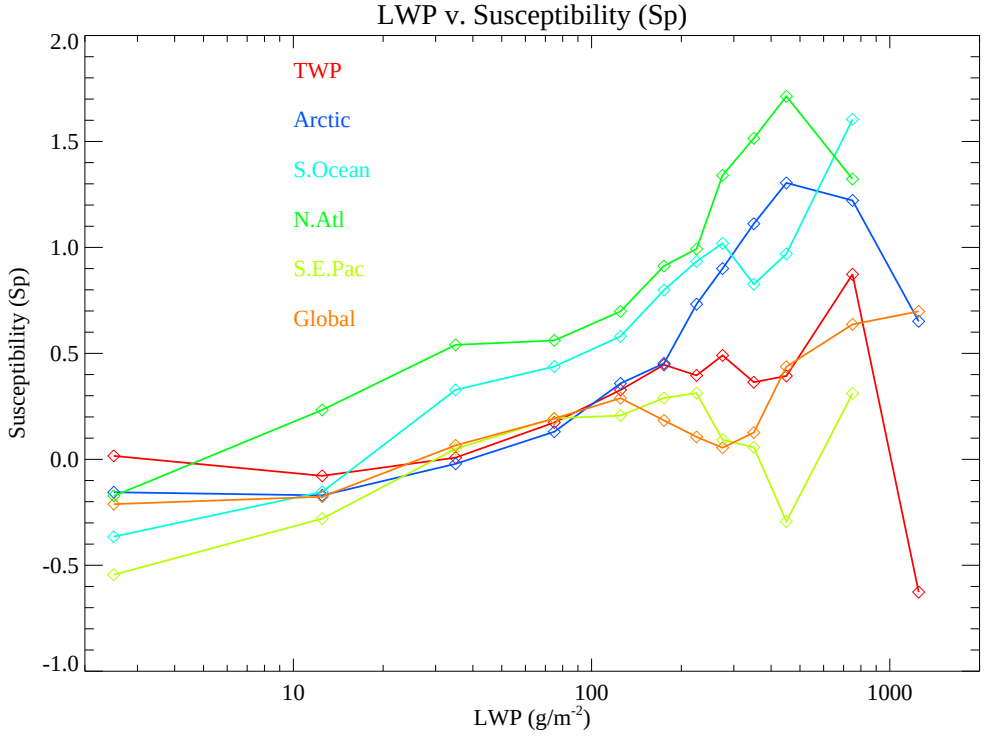

Fig. 7. Regional averages of precipitation susceptibility (S_p) as described in the text for different regions (colors, see Figure 5 for description) binned by LWP.

Table 2. Description of global simulations used in this study.

Name	Description
Base	Base simulation
Au/10	Autoconversion rate divided by 10x
Ac*10	Accretion rate increased by 10x
QrScl$^{0.75}$	Scaled rain mixing ratio for accretion
dT/4	Physics time step reduced from 1800 to 450s
Base2	Base simulation 2 (different code base)
AcAu2	Ac*10 and Au/10

CRE is the difference between the top of atmosphere flux for all sky and clear sky conditions, for both shortwave (SWE) and long-wave (LWE). Alternatively, the change in clear sky shortwave flux (dFSC) is a measure of the direct scattering from aerosols, so the indirect effect (ACI) can also be RFP - dFSC. In general these measures are similar.

First we note that there are correlations between the change in short wave cloud radiative effect (dSWE) and the mean LWP. An examination of differences in each simulation indicates that the magnitude of the ACI as defined by dCRE scale roughly inversely with the mean liquid water path: the largest radiative effect (and change in cloud radiative effect) occurs for the boosted accretion (Ac*10) simulation, which also has the smallest mean LWP, the largest change in LWP (Table 3), and the largest percent change in the cloud drop number (CDN). Similar conclusions can be drawn from defining ACI = dR - dFSC.

The results illustrate a fairly narrow range of changes in CRE due to aerosol cloud interactions, with a spread between simulations on the order of $\sim$25%. The change in cloud radiative effect varies slightly, despite large differences (a factor of 2) in mean LWP in Table 3. The ACI defined by dSWE is correlated with the mean LWP (r^2= 0.85) and dLWP (r^2= 0.85). Platnick and Twomey (1994) note that low LWP clouds have higher albedo susceptibility ($\partial ln[\alpha]/\partial ln[CDN]$), and these radiative effects are seen here: lower mean LWP results in higher SW effects. The liquid water path changes themselves are fairly easy to explain. Decreasing autoconversion (Au/10) increases mean present day LWP substantially. Increasing accretion (Ac*10) decreases LWP. The QrScl experiment is a combination of

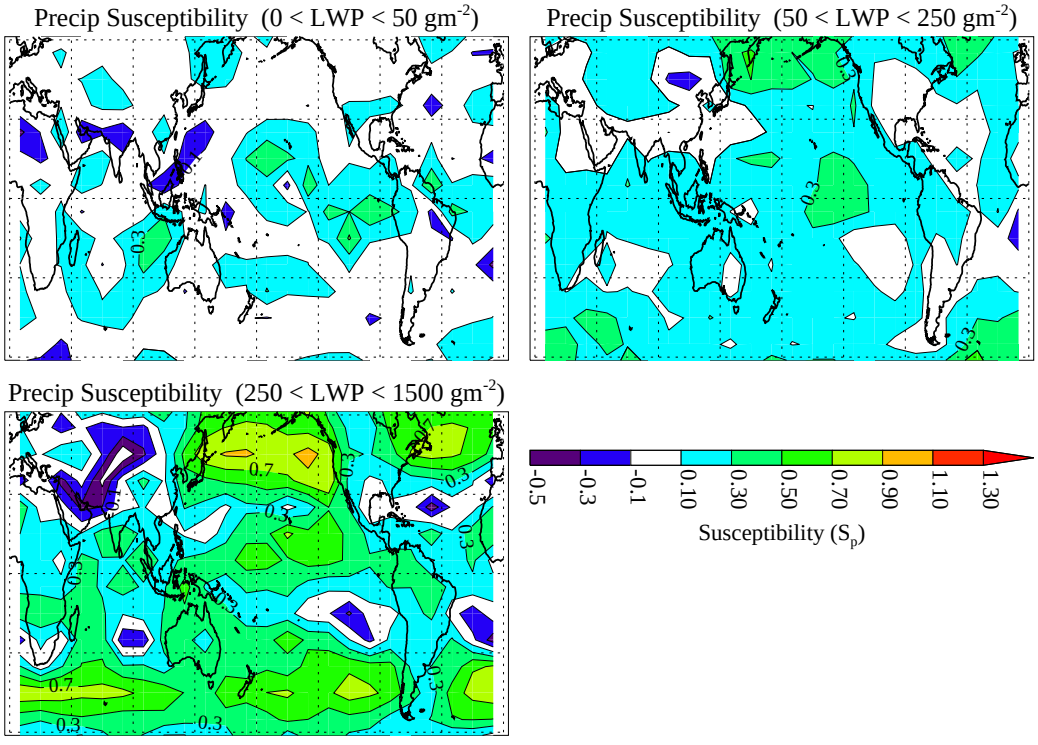

Fig. 8. Maps of precipitation susceptibility (S_p) for base model for 3 different LWP ranges. A) 0–50 gm^{-2}, B) 50–250gm^{-2} and C) 250–1500gm^{-2}.

Table 3. Table of radiative property changes (year 2000-1850) from simulations. Illustrated are change in top of atmosphere radiative fluxes (R), net cloud radiative effect (CRE) as well as the long-wave effect (LWE) and shortwave effect (SWE) components, the change in clear-sky shortwave radiation (FSC), ice water path (IWP) and year 2000 liquid water path (LWP). Also shown are changes to in-cloud ice number concentration (INC) and column liquid drop number (CDN)

Run	*d*R Wm^{-2}	*d*CRE Wm^{-2}	*d*LWE Wm^{-2}	*d*SWE Wm^{-2}	*d*FSC Wm^{-2}	LWP gm^{-2}	*d*LWP gm^{-2}	*d*INC L^{-1}	*d*CDN 10^{10} cm^{-2}
Base	-1.40	-1.06	0.48	-1.54	-0.46	44.0	3.1 (7%)	6.4 (13%)	0.62 (40%)
Au/10	-1.31	-1.01	0.40	-1.41	-0.36	65.0	3.2 (5%)	5.9 (12%)	0.76 (35%)
Ac*10	-1.37	-1.22	0.70	-1.92	-0.34	28.1	2.7 (10%)	9.1 (17%)	0.41 (48%)
QrScl	-1.18	-1.00	0.68	-1.68	-0.35	31.2	1.4 (5%)	9.5 (17%)	0.42 (41%)
dT/4	-1.37	-1.01	0.36	-1.37	-0.61	49.0	3.2 (7%)	7.8 (8%)	0.61 (36%)
Base2	-1.55	-1.25	0.43	-1.68	-0.32	44.4	3.2 (7%)	6.6 (12%)	0.64 (41%)
AcAu2	-1.21	-1.10	0.61	-1.71	-0.25	44.4	2.4 (5%)	7.9 (14%)	0.55 (35%)

increasing the accretion rate through scaling the rain mixing ratio (reducing LWP) and decreasing autoconversion to increase it again: the overall effect is to decrease LWP from the base case. The dT/4 case has 10% higher LWP than the base simulation: this is expected since a shorter time step means less time for large amounts of cloud water to build up after macrophysics but before microphysics, thus microphysical process rates (sinks) are smaller, explaining the increase in LWP. As shown by Golaz et al. (2011), these changes in LWP may affect ACI since changing A_u and A_c affect LWP as well

as ACI. We control for this by looking at an additional simulation: the AcAu2 simulation has the same mean LWP as its control, Base2 (Table 3). ACI in this simulation is ∼15% lower than Base2, indicating boosting accretion over autoconversion does have effects on ACI independent of mean LWP. Note that the change in LWP in AcAu2 is lower than Base2, so that the SW radiative ACI seems to be related to dLWP. Autoconversion is too large, and accretion increases less with LWP.

Figure 9 illustrates the process rates in the different simulations. For increased accretion (Ac*10) and scaled diagnostic rain (QrScl$^{0.75}$), the A_c/A_u ratio is significantly reduced, and the slope with LWP is slightly reduced (Figure 9 A). This occurs because of a reduction in accretion with respect to LWP, even if the accretion is boosted (Ac*10 and QrScl$^{0.75}$), as in the steady state model. In the GCM, boosting accretion tends decrease LWP (shifting the curves to the left in Figure 9 A). The estimates based on VOCALS observations are also included in Figure 9 (blue), and the behavior of the model is very different than the observations for all cases, as noted for the base case in Figure 5.

There are significant changes in the precipitation susceptibility in the different simulations with altered process rates. Figure 10 illustrates the susceptibility for different simulations. The CAM5 base simulation (solid) features increasing susceptibility globally and in the VOCALS region up to an LWP of about 800 gm^{-2}. The reduced autoconversion (Au/10) case has increased susceptibility at higher LWPs. However, for the increased accretion cases (Ac*10 and QrScl$^{0.75}$), with lower slope to the Accretion/Autoconversion ratio (Figure 9 A), the susceptibility is reduced significantly and approaches zero for higher liquid water paths. The simulation with smaller time step only (dT/4) features the strongest increase in susceptibility. It is not clear that this affects the radiative impact of the aerosol cloud interactions (Table 3) significantly. The QrScl$^{0.75}$ simulation does have 20% or so lower ACI, and has the lowest susceptibility at high LWP. The A_u/R ratio in these simulations (not shown) does not appear to predict the precipitation susceptibility (S_p), in contrast to the steady state model (Figure 3 B and D).

6 Discussion/Conclusions

Autoconversion and accretion processes are dominant in controlling the liquid water path with bulk 2 moment microphysics in the GCM. This is seen in microphysical budget calculations (Figure 1) as well as in sensitivity tests, where altering these process rates has direct impacts on liquid water path (Table 3). The mean state of the GCM climate (base LWP) is quite sensitive to the formulation of the microphysical process rates: accretion and autoconversion have direct impacts on sources and sinks of liquid. The coupling of these processes to the rest of the model, by altering the time step, also impacts the mean state. These results are consistent with previous work, but use analysis of observations and a steady state model.

The steady state model (Figures 2 and 3) reproduces relationships found in detailed Large Eddy Simulations (LES) with respect to these microphysical processes. Accretion increases with respect to autoconversion as LWP increases. Autoconversion as a proportion of rain decreases at higher LWP, while accretion's contribution increases. The formulation uses the same semi-empirical formulations for autoconversion and accretion as in the global model. The steady state model has very different behavior when used with a modified formulation of accretion to reflect the behavior of diagnostic precipitation in the GCM. Here the autoconversion contribution to rain remains high as LWP increases, as in the GCM. Further adjusting process rates can partially recover the initial behavior with higher levels of accretion relative to autoconversion in the unmodified steady state model. The susceptibility of precipitation to drop number decreases with liquid water path in the unmodified steady state model, but remains constant at high liquid water paths with the assumptions about rain used in the GCM, consistent with the A_u/R relationship.

The behavior of the CAM5 GCM is similar to the steady state model with the modified accretion formulation. In the model, autoconversion is much more important, and increases relative to accretion at higher liquid water paths (Figure 5). The microphysical behavior seems fairly consistent across regions. The proportion of rain from autoconversion also increases as LWP increases (Figure 6). Because autoconversion is dependent strongly on drop number, it links aerosols to cloud lifetime increases and the decrease in precipitation. Susceptibility increases with LWP in CAM up to large values of LWP (Figure 7), and higher susceptibility is found in regions with higher LWP (Figure 8), and lower A_c/A_u ratios (Figure 4F).

Posselt and Lohmann (2008) showed that diagnostic rain leads to overestimating the importance of autoconversion and Wang et al. (2012) showed that the A_u/R ratio correlated with the sensitivity of LWP to aerosols. Here we illustrate that using a 'diagnostic-like' formulation in the steady state model can drastically shift the rain formation from accretion to autoconversion. Attempting to correct the GCM by boosting accretion (as in Ac*10 or QrScl$^{0.75}$), the GCM still has a difficult time capturing the expected behavior of the A_c/A_u ratio (as evidenced by how the A_c/A_u ratio for QrScl$^{0.75}$ is actually lower than the Base run in Figure 9 A). While the tendency for increasing autoconversion with LWP is still present in the GCM, susceptibility does appear to be modified (reduced) when the process rates are modified (Figure 10), or when the time step is shortened. In the GCM, spatial changes in the accretion/autoconversion ratio (Figure 4) appear to be reflected in the precipitation susceptibility (Figure 8), but this is not apparent in the global averages in Figure 9, likely due to the averaging across regimes.

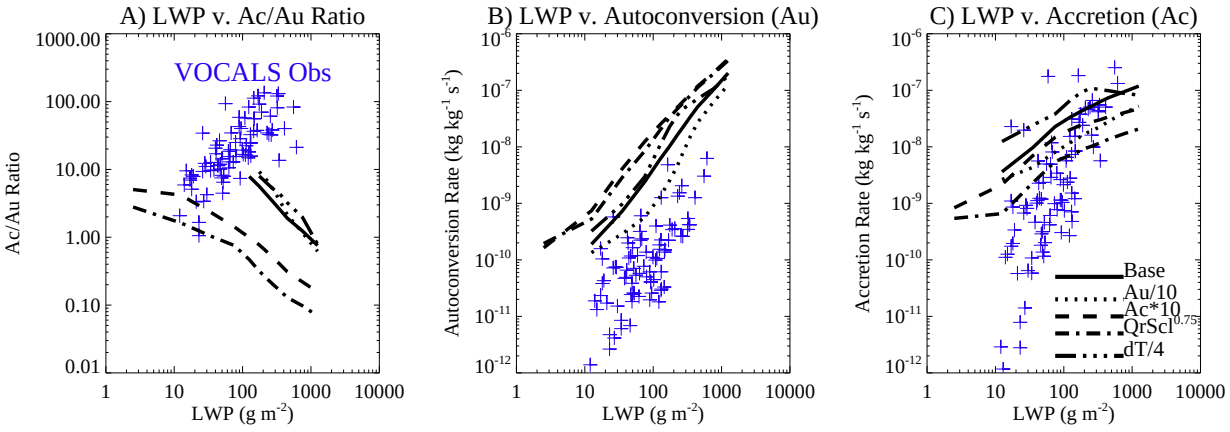

Fig. 9. Regional and global averages of vertically averaged (A) Accretion/Autoconversion (A_c/A_u) ratio v. LWP , (B) Autoconversion (A_u) rate v. LWP and (C) Accretion (A_c) rate v. LWP. Simulations are described in Table 2. Base CAM5 (solid), Au/10 (dotted), Ac*10: (dashed), QrScl$^{0.75}$ (Dot Dashed) and dT/4 (triple dot-dash). Also shown are observational estimates (blue crosses) from VOCALS aircraft flights as described in the text.

In the GCM, the susceptibility does not correlate with the A_c/A_u as strongly as in the steady state model (when comparing DiagQr and DiagQr$^{0.5}$ in Figure 3). S_p seems related to the slope of the A_c/A_u ratio. Comparing Figure 9 and Figure 10, the runs with higher A_c/A_u ratios do not have lower susceptibilities at high LWP as expected. QrScl$^{0.75}$ and Ac*10 cases have lower LWP and lower A_c/A_u ratio, but reduced S_p at high LWP. Note that this might be related to the LWP: in the steady state model base case in Figure 3, the A_c/A_u ratio of the base case increases substantially, but susceptibility doesn't really respond until at around LWP$\sim$500 gm^{-2}. This highlights the complexity of the interactions in the GCM, where multiple processes are affecting LWP in multiple regimes. There are also ice processes in many GCM regions that complicate the analysis.

The radiative Aerosol-Cloud Interactions (ACI, also called indirect effects) are sensitive to these process rate changes, but the changes may be convolved with differences in base state LWP, similar to Golaz et al. (2011). The larger radiative impacts of cloud-aerosol interactions occur for the largest percent changes in liquid water path and drop number in the Ac*10 simulation with enhanced accretion. When the steady state model diagnostic rain 'correction' is applied to accretion in the GCM (QrScl$^{0.75}$), ACI is reduced by 20% between this calculation and the enhanced accretion case (Ac*10) with similar mean LWP (Table 3). Or stated another way: with half the LWP of the Base case, essentially the same ACI is predicted. A different experiment with reduced autoconversion and increased accretion (AcAu2) to maintain the same LWP as the base case also reduced ACI by $\sim$15%. This is consistent with the reduced susceptibility in Figure 10.

We conclude that the simple steady state model reproduces many of the feature seen in cloud resolving (LES) models and observations. The steady state model can also be made to produce similar relationships as in the global model: which we attribute to the differences between prognostic and diagnostic precipitation. It does not appear as if the bulk, semi-empirical formulations of the process rates derived from fits to a CRM by Khairoutdinov and Kogan (2000) cause the relative increase in Autoconversion over Accretion with higher LWP, since this does not occur in the steady state model with these formulations. This is an important conclusion for many scales of modeling. It appears that radiative ACI in the GCM may be sensitive to the formulation of the diagnostic precipitation. CAM5 is conceptually similar to many other GCMs in how it treats cloud microphysics and aerosols, so these results might be generally applicable across models. Possible sensitivities to LWP confound this interpretation, consistent with radiative effects (Platnick and Twomey, 1994) and recent GCM tuning experiments (Golaz et al., 2011). It appears that reductions of ACI of 20% or so, and decreases in precipi-

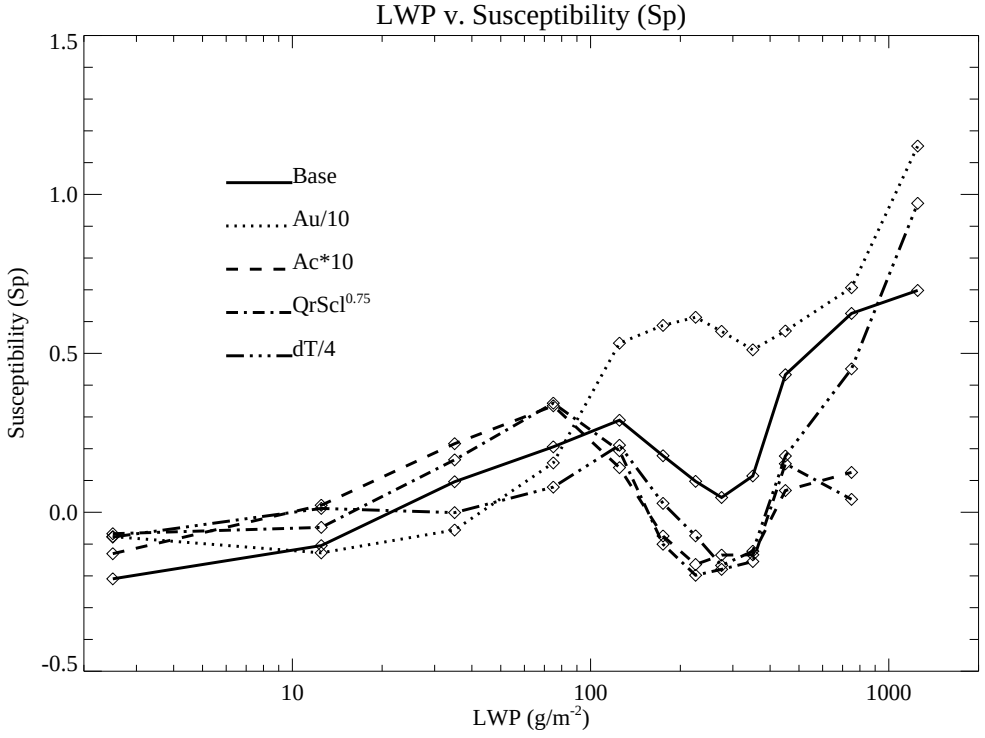

Fig. 10. Global average Precipitation Susceptibility (S_p) as defined in the text. Simulations are described in Table 2. Base CAM5 (solid), Au/10 (dotted), Ac*10: (dashed), QrScl$^{0.75}$ (Dot Dashed) and dT/4 (triple dot-dash).

tation susceptibility (Figure 10) result from these process rate changes.

These conclusions will need further testing in both GCM and off-line frameworks, including in other GCMs. We are continuing this research both by extending the Morrison and Gettelman (2008) microphysics scheme to include prognostic precipitation. The possibility also exists that the numerics may have an impact. The combination of the diagnostic precipitation assumption with relatively long time steps (20 min, with 10 min iterations for precipitation), as well as coarse vertical grid spacing (500–1000m in the free troposphere) may impact the simulations. We intend to explore these numerical issues further with a detailed 1d model as a step on the way to more robust formulations of microphysics that work across different time and space scales.

Acknowledgements. Computing resources were provided by the Climate Simulation Laboratory at National Center for Atmospheric Research (NCAR) Computational and Information Systems Laboratory. NCAR is sponsored by the U.S. National Science Foundation (NSF). The authors were supported by a Climate Process Team grant from NSF, AGS-0968657.

References

Ackerman, A. S., Kirkpatrick, M. P., Stevens, D. E., and Toon, O. B.: The impact of humidity above stratiform clouds on indirect aerosol climate forcing, Nature, 432, 1014–1017, 2004.

Albrecht, B. A.: Aerosols, cloud microphysics and fractional cloudiness, Science, 245, 1227–1230, 1989.

Boucher, O. and Lohmann, U.: The sulfate-CCN-cloud albedo effect. A sensitivity study with two general circulation models, Tellus, 47B, 281–300, 1995.

Feingold, G. and Siebert, H.: Cloud–Aerosol Interactions from the Micro to the Cloud Scale, in: Clouds in the Perturbed Climate System, edited by Heintzenberg, J. and Charlson, R. J., MIT Press, 2009.

Gettelman, A., Morrison, H., and Ghan, S. J.: A new two-moment bulk stratiform cloud microphysics scheme in the NCAR Community Atmosphere Model (CAM3), Part II: Single-Column and Global Results, J. Clim., 21, 3660–3679, 2008.

Gettelman, A., Liu, X., Ghan, S. J., Morrison, H., Park, S., Conley, A. J., Klein, S., Boyle, J., Mitchell, D. L., and Li, J.-L. F.: Global Simulations of Ice nucleation and Ice Supersaturation with an Improved Cloud Scheme in the Community Atmosphere Model, J. Geophys. Res., 115, doi:10.1029/2009JD013797, 2010.

Gettelman, A., Kay, J. E., and Shell, K. M.: The Evolution of Climate Feedbacks in the Community Atmosphere Model, J. Clim., 25, 1453–1469, doi:10.1075/JCLI-D-11-00197.1, 2012.

Golaz, J.-C., Saltzmann, M., Donner, L. J., Horowitz, L. W., Ming, Y., and Zhao, M.: Sensitivity of the aerosol indirect effect to subgrid variability in the cloud parameterization of the GFDL Atmosphere General Circulation Model AM3, J. Clim., 24, 3145–3160, doi:10.1175/2010JCLI3945.1, 2011.

Guo, H., Golaz, J.-C., and Donner, L. J.: Aerosol effects on stratocumulus water paths in a PDF-based parameterization, Geophys. Res. Lett., 38, doi:10.1029/2011GL048611, http://dx.doi.org/10.1029/2011GL048611, 2011.

Jiang, H., Feingold, G., and Sorooshian, A.: Effect of Aerosol on the Susceptibility and Efficiency of Precipitation in Warm Trade Cumulus Clouds, J. Atmos. Sci., 67, 3526–3540, 2010.

Khairoutdinov, M. F. and Kogan, Y.: A new cloud physics parameterization in a large-eddy simulation model of marine stratocumulus, Mon. Weather Rev., 128, 229–243, 2000.

Lamarque, J.-F., Bond, T. C., Eyring, V., Granier, C., Heil, A., Klimont, Z., Lee, D., Liousse, C., Mieville, A., Owen, B., Schultz, M. G., Shindell, D., Smith, S. J., Stehfest, E., Van Aardenne, J., Cooper, O. R., Kainuma, M., Mahowald, N., McConnell, J. R., Naik, V., Riahi, K., and van Vuuren, D. P.: Historical (1850–2000) gridded anthropogenic and biomass burning emissions of reactive gases and aerosols: methodology and application, Atmos. Chem. Phys., 10, 7017–7039, doi:10.5194/acp-10-7017-2010, http://www.atmos-chem-phys.net/10/7017/2010/, 2010.

Liu, X. et al.: Towards a Minimal Representation of Aerosol Direct and Indirect Effects: Model description and evaluation, Geosci. Model Dev., 5, 709–735, doi:10.5194/gmd-4-709-2012, 2012.

Martin, G. M., Johnson, D. W., and Spice, A.: The measurement and parameterization of effective radius of droplets in warm stratocumulus clouds, J. Atmos. Sci., 51, 1823–1842, 1994.

Morrison, H. and Gettelman, A.: A new two-moment bulk stratiform cloud microphysics scheme in the NCAR Community Atmosphere Model (CAM3), Part I: Description and Numerical Tests, J. Clim., 21, 3642–3659, 2008.

Murphy, D. M., Solomon, S., Portmann, R. W., Rosenlof, K. H., Forster, P. M., and Wong, T.: An observationally based energy balance for the Earth since 1950, J. Geophys. Res., 114, doi:10.1029/2009JD12105, 2009.

Neale, R. B. et al.: Description of the NCAR Community Atmosphere Model (CAM5.0), Tech. Rep. NCAR/TN-486+STR, National Center for Atmospheric Research, Boulder, CO, USA, 2010.

Platnick, S. and Twomey, S.: Determining the susceptibility of cloud albedo to changes in droplet concentration with the Advanced Very High Resolution Radiometer, J. Applied Met., 33, 1994.

Posselt, R. and Lohmann, U.: Introduction of prognostic rain in ECHAM5: design and single column model simulations, Atmos. Chem. Phys., 8, 2949–2963, 2008.

Quaas, J., Boucher, O., Bellouin, N., and Kinne, S.: Satellite-based estimate of the direct and indirect aerosol climate forcing, JGR, 113, doi:10.1029/2007JD008962, 2008.

Ramanathan, V., Crutzen, P. J., Kiehl, J. T., and Rosenfeld, D.: Aerosols, climate and the hydrologic cycle, Science, 294, 2119–2124, 2001.

Rosenfeld, D., Lohmann, U., Raga, G. B., O'Dowd, C. D., Kulmala, M., Fuzzi, S., Reissell, A., and Andreae, M. O.: Flood or Drought: How do Aerosols Affect Precipitation, Science, 321, 1309–1313, 2008.

Sorooshian, A., Feingold, G., Lebsock, M. D., Jiang, H., and Stephens, G. L.: On the precipitation susceptibility of clouds to aerosol perturbations, Geophys. Res. Lett., 36, doi:10.1029/2009GL038993, 2009.

Stevens, B. and Seifert, A.: Understanding microphysical outcomes of microphysical choices in simulations of shallow cumulus convection, J. Meteor. Soc. Japan, 86, 143–162, 2008.

Taylor, K. E., Stouffer, R. J., and Meehl, G. A.: An Overview of CMIP5 and the Experimental Design, in press, Bull. Amer. Met. Soc, 2012.

Terai, C. R., Wood, R., Leon, D. C., and Zuidema, P.: Does precipitation susceptibility vary with increasing cloud thickness in marine stratocumulus?, Atmos. Chem. Phys., 12, 4567–4583, doi:10.5194/acp-12-4567-2012, http://www.atmos-chem-phys.net/12/4567/2012/, 2012.

Twomey, S.: The Influence of Pollution on the Shortwave Albedo of Clouds, J. Atmos. Sci., 34, 1149–1152, 1977.

Wang, M. et al.: Constraining cloud lifetime effects of aerosols using A-Train Satellite observations, Geophys. Res. Lett., 39, doi:10.1029/2012GL052204, 2012.

Wood, R.: Drizzle in stratiform boundary layer clouds. Part II: Microphysical aspects, J. Atmos. Sci., 62, 3034–3050, 2005.

Wood, R., Kubar, T. L., and Hartmann, D. L.: Understanding the Importantce of Microphysics and Macrophysics for Warm Rain in Marine Low Clouds. Part II: Heuristic Models of Rain Formation, J. Atmos. Sci., 66, 2973–2990, doi:10.1175/2009JAS3072.1, 2009.

Wood, R. et al.: The VAMOS Ocean-Cloud-Atmosphere-Land Study Regional Experiment (VOCALS-REx): goals, platforms, and field operations, Atmos. Chem. Phys., 11, 627–654, doi:10.5194/acp-11-627-2011, 2011.

Zhang, G. J. and McFarlane, N. A.: Sensitivity of climate simulations to the parameterization of cumulus convection in the Canadian Climate Center general circulation model, Atmos. Ocean, 33, 1995.